Uncovering the intrinsic geometry from the atomic pair distribution function of nanomaterials

Ming Lei
Department of Biochemistry, Brandeis University, 415 South Street, Waltham, Massachusetts 02453, USA

Adam M. R. de Graff and M. F. Thorpe
Department of Physics, Bateman Physical Sciences PSF 359, Arizona State University, Tempe, Arizona 85287-1504, USA

Stephen A. Wells
Department of Physics and Centre for Scientific Computing, University of Warwick, Gibbet Hill Road, Coventry CV4 7AL, United Kingdom

Asel Sartbaeva
Inorganic Chemistry Laboratory, University of Oxford, South Parks Road, Oxford OX1 3QR, United Kingdom
(Received 27 January 2009; revised manuscript received 18 May 2009; published 30 July 2009)

Atomic pair distribution functions are useful because they have an easy intuitive interpretation and can be obtained both experimentally and from computer-generated structure models. For bulk materials, atomic pair distribution functions are solely determined by the intrinsic atomic geometry, i.e., how atoms are positioned with respect to one another. For a nanomaterial, however, the atomic pair distribution function also depends on the shape and size of the nanomaterial. A modified form of the radial distribution function is discussed that decouples shape and size effects from intrinsic effects so that nanomaterials of any shape and size, sharing a common atomic geometry, map onto a universal curve, by using a form factor. Mapping onto this universal curve allows differences in the intrinsic atomic geometry of nanomaterials of various shapes and sizes to be directly compared. This approach is demonstrated on nanoscale amorphous and crystalline silica models. It is shown how form factors can be computed for arbitrary shapes and this is illustrated for tetrahedral nanoparticles of vitreous silica.

DOI: 10.1103/PhysRevB.80.024118 PACS number(s): 61.43.Bn

I. INTRODUCTION

The atomic pair distribution function describes the distance-dependent density distribution of a material as viewed from an average atom. It links microscopic atomic placements with macroscopic experimental observables such as pressure, compressibility, energy, and phase transitions.[1] It can be determined either experimentally by taking the Fourier transform of neutron or x-ray diffraction or from computer-generated structure models.[2] In this paper we will focus on the radial distribution function (RDF), that is closely related to the pair distribution function. A comparison between the measured and computed RDFs provides insight into the structural origin of experimental observables. For example, RDFs have been used to probe the architecture of novel amorphous and porous materials,[3] illustrate the phase transition across the optimal doping of superconducting materials,[4] and detect randomness in periodic superlattices.[5]

The computation of an RDF consists essentially of counting the number of atoms within a thin shell a given distance away from an average atom. In general, it is affected by two types of structural properties. The first type relates to the intrinsic geometry of the atomic network, i.e., the average coordination of each atom, the distortion of bond lengths and bond angles, and the randomness of the atomic network. These properties influence how atoms are placed with respect to each other. They determine the positions, intensities, widths, and overlaps of the peaks in the RDF. The second type relates to spatial confinement, i.e., the shape and the size of the material sample. They determine the envelope of the RDF.

Infinite in all directions, a bulk material has neither shape nor size. Thus the RDF of a bulk material is only determined by the intrinsic geometry of its atomic network. In contrast, the RDF of a nanomaterial is a function of its shape and size in addition to the atomic geometry.[6] A nanomaterial, by definition, is smaller than 1 μm in at least one dimension and thus a non-negligible fraction of the atoms are on or close to the surface of the material. These surface atoms are surrounded partially by the material and partially by vacuum. The density distributions viewed from these atoms differ from those viewed from the deeply buried atoms. Since the RDF of a nanomaterial is the average of the density distributions viewed from all atoms, the RDF entangles the contributions from both the intrinsic atomic geometry and the spatial confinement.

The determination of the shape and size of a nanomaterial are usually not the goal of RDF analysis, as they can be obtained from experimental techniques such as small-angle x-ray scattering (Ref. 7) and transmission electron microscopy.[8] The main research interests here are the determination of the intrinsic atomic geometry of a nanomaterial and its deviation from that of the corresponding bulk material. It is therefore desirable to compute the RDF of a nanomaterial in such a way that the atomic geometry is decoupled from the spatial confinement effects. Most conventional forms of RDFs discussed in textbooks and the literature, however, do not take spatial confinement factors into consideration. This is not a surprise, as most of the RDF theory was developed in the days when bulk materials were the main if not the sole research subjects in condensed-matter physics

and materials science. With ever-growing interests in nanomaterials, it is desirable to have a form of RDF, that is, free of the spatial confinement effects. This form of RDF causes the atomic distribution of nanomaterials with the same intrinsic atomic geometry but different shapes and sizes to map onto a universal curve, thus allowing deviations in the atomic geometry due to distortions from boundary effects to be more easily compared.

II. THEORY AND METHODOLOGY

Under the general name of pair distribution functions, several sets of functions are used in the powder-diffraction community.[9] The nomenclature used in this paper follows that of the book by Warren.[2] The function, that is found directly from the structure factor $S(Q)$ is the reduced pair distribution function $G(r)$. The form of $G(r)$ is related to $S(Q)$ according to

$$G(r) = \frac{2}{\pi}\int_0^\infty Q[S(Q)-1]\sin QrdQ. \tag{1}$$

This commonly used equation is somewhat misleading, as it assumes that $S(Q)$ does not contain contributions from small-angle scattering (SAS), a point discussed in more detail later in this section. For bulk materials

$$G(r) = 4\pi r\rho_0\left(\frac{R(r)}{4\pi r^2\rho_0} - 1\right) \tag{2}$$

which needs to be modified for nanomaterials if it is to fluctuate about zero at large r. Equation (2) is expressed in terms of $R(r)$, the RDF, defined as

$$R(r) = \frac{1}{N}\sum_{ij}\frac{w_i w_j}{\langle w\rangle^2}\delta(r-r_{ij}). \tag{3}$$

The RDF is a more intuitive function than $G(r)$ and describes the number of atoms within a thin spherical shell between r and $r+dr$ viewed from an average atom. Here w_i are the atomic weight factors suitable for x-ray or neutron scattering and $\langle w\rangle = \Sigma_i w_i/N$ is averaged over all sites in the nanomaterial. The quantity r_{ij} indicates the interatomic distance between the ith and the jth atoms and N the total number of atoms in the material. The sum in Eq. (3) is over all atom pairs. Therefore the integration of the RDF over the whole valid range of r is N. An RDF is simply the unnormalized weighted histogram of the interatomic distances. Given a structure model, it is the most straightforward distribution function to compute. The derivation of a universal function characteristic of any given material free of finite-size effects will be performed using $R(r)$ due to its intuitive nature. The universal function is then expressed in terms of $G(r)$, the function found directly from experiment.

For a bulk material, the RDF $R(r)$ approaches $4\pi r^2\rho_0$ at large distances, where ρ_0 is the average density of the material. A reduced RDF (RRDF) $P(r)$ is frequently used in the literature to normalize out the long-distance trend

$$P_b(r) = \frac{R(r)}{4\pi r^2\rho_0} \tag{4}$$

so that at large distances, this function approaches 1. The subscript b indicates that the RRDF approaches 1 only for bulk systems. The average density in a spherical shell of radius r fluctuates around ρ_0 with an amplitude that decreases with increasing r. A crystal can be shown to display the most gradual decrease in peak amplitude, decreasing as $1/r$ because of lingering long-range effects which are absent in amorphous materials.[10]

It is only in bulk material that the RDF actually approaches $4\pi r^2\rho_0$ at large distances. For a nanomaterial, the large distance limit of the RDF is determined by its shape and size. For example, if the nanomaterial is an infinite sheet (finite in one dimension), the RDF tends to $2\pi r\rho_0$, where ρ_0 is the effective layer density. If the nanomaterial is an infinite rod (finite in two dimensions), the RDF tends to $2\rho_0$, where here ρ_0 is the effective line density. If the nanomaterial is finite in all three dimensions, the RDF is exactly zero beyond the longest distance within the material. Consequently, the RRDFs computed according to Eq. (4) have very different asymptotic behavior depending on the size and shape of the nanomaterial. Specifically, they are proportional to $1/r$, $1/r^2$, and 0 for nanomaterials that are finite in one, two, and three dimensions, respectively. In general, the distribution functions defined in Eqs. (3) and (4) are not directly comparable for nanomaterials of different shape and size.

The RRDF of a bulk material has the nice feature that it converges to the constant of 1 in the long-distance limit. RRDFs of different bulk materials can thus be directly compared, as they have the same baseline. For a nanomaterial, it is also desirable to have a similarly defined distribution function that has the same flat baseline of unity at large distances (for nanomaterials finite in all three dimensions within the valid distance range) regardless of the shape and size of the material. Such a function should be independent of spatial confinement effects and depend only on the intrinsic atomic geometry of the material so that the latter can be easily compared between different nanomaterials and between a nanomaterial and its bulk counterpart.

The reason the RRDF as defined by Eq. (4) trends away from unity for a material bounded in one or more dimensions is that a spherical shell of radius r placed about a typical atom can have part its surface outside of the bounded material, whereas this can never occur for a bulk material. The RDF of a bounded material is therefore always less than its bulk equivalent, causing the RRDF to trend below unity. For the infinite sheet and infinite rod, their long-distance trends indicate that the average fraction of the spherical shell lying outside the boundary of the material decreases as $1/r$ and $1/r^2$, respectively. The function that describes the distance dependence of this fraction has been called the characteristic function of the shape[6] or the nanoparticle form factor[11] in the literature, but for clarity it will simply be referred to as the shape factor $f(r)$. If the RRDF is instead defined as

$$P(r) = \frac{R(r)}{4\pi r^2\rho_0 f(r)}, \tag{5}$$

the distance dependence of $R(r)$ is matched by that of $f(r)$, causing this more general RRDF to fluctuate about unity for

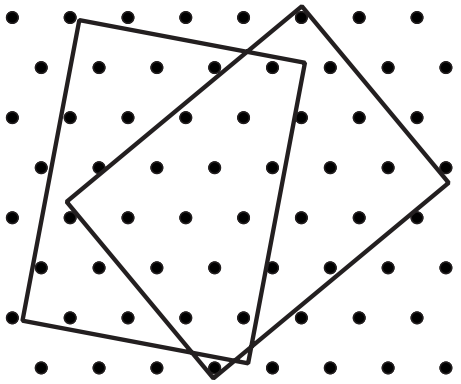

FIG. 1. The statement that $R(r)=R_b(r)f(r)$ is equivalent to averaging the RDFs of the ensemble of nanomaterials cut from the bulk at all locations and orientations with equal probability. Two such random locations and orientations are displayed for the case of rectangular nanomaterials cut from a triangular lattice.

a nanomaterial of any shape and size, as desired. The general RRDF $P(r)$ is an invariant depending only on the intrinsic atomic geometry of the bulk material and not on the shape and size of possible boundaries.

Rewriting Eq. (5) as $R(r)=4\pi r^2\rho_0 P(r)f(r)$ and recognizing that $4\pi r^2\rho_0 P(r)$ is the RDF $R_b(r)$ of the bulk material, Eq. (5) is equivalent to

$$R(r) = R_b(r)f(r). \tag{6}$$

The RDF of an undistorted nanomaterial can therefore be expressed as the product of two independent distributions, one containing only information regarding the intrinsic atomic geometry of the material and the other describing only the effects of spatial confinement. From Eq. (6), $f(r)$ for a nanomaterial can also be interpreted as describing the probability that two randomly chosen points from the bulk material separated by a distance r will be found within the boundary of the nanomaterial. The nanomaterial can be imagined to have been cut from the bulk material without undergoing deformation or reconstruction. Unfortunately, knowing the bulk material and the boundary describing the shape and size does not uniquely specify the nanomaterial, as it could be cut from the bulk at any location and orientation, each giving a different realization of the nanomaterial with a different RDF, as shown in Fig. 1. The RDFs of the two cuts in Fig. 1 not only contain peaks of different amplitude but the rightmost cut contains a peak due to the atoms in the upper and lower corners, that is, entirely absent in the first cut. The apparent dilemma is due to the fact that $f(r)$ depends only on a nanomaterial's shape and size and is defined for an object of uniform density (see Appendix), while here the density is inhomogeneous at the atomic level. The problem is resolved and Eq. (6) made exact if cuts at *all locations and orientations* are sampled with equal probability and $R(r)$ is the average RDF of the ensemble. For any sample of nanomaterials that does not contain an equal representation of all boundary locations and orientations, as is the case for nonspherical nanomaterials with preferential directions of growth that correlate with the underlying atomic geometry,[12] Eq. (6) is only an approximation for the average RDF of the sample. As the shape factor $f(r)$ is independent of the density distribution within the boundary, it can be calculated by finding the RDF $R^u(r)$ of a material of uniform density ρ_0 (the superscript u stands for uniform density) of the desired shape and size, and dividing it by the RDF of the uniform bulk, $R_b^u(r)=4\pi r^2\rho_0$. The general RRDF for infinite or bounded materials can therefore be written as

$$P(r) = \frac{R(r)}{R^u(r)} = \frac{R(r)}{R_b^u(r)f(r)} = \frac{R(r)}{4\pi r^2\rho_0 f(r)}. \tag{7}$$

For bulk materials, $f(r)\equiv 1$ and the RRDF given by Eq. (7) reduces to Eq. (4). Therefore, Eq. (7) is an extension of an already widely used distribution function. *The RRDF* $P(r)$ is a means *of plotting RDF data such that data for nanomaterials of all shapes and sizes with a common atomic arrangement fall on a single curve, allowing differences in their intrinsic atomic geometry to be more readily compared.* Although strictly speaking, the shape independence of $P(r)$ in Eq. (7) is only true after averaging over nanomaterials with all possible locations and orientations with respect to the bulk material, in practice it can be used to approximate the RDF of a single realization of the nanomaterial, except at the very largest spanning distances within the nanomaterial, as discussed in Sec. IV. Care is needed when the nanomaterials are highly nonspherical, as, for example, in needles, for which the deviations from spherical symmetry are strongly correlated with asymmetries of the atomic lattice.[12] For nanomaterials, where all the spanning lengths are at the same length scales, deviations in $P(r)$ from that of the bulk material can be ascribed to structural changes from the bulk due to surface relaxation and structural rearrangement.[12]

For nanomaterials, $R^u(r)$ and the shape factor $f(r)$ depend on the shape and size of the material. Analytic expressions of $R^u(r)$ are available for some simple geometrical shapes (see Appendix) and all others of interest can be computed numerically by creating a histogram of the distances between pairs of points placed randomly within the boundary of the nanomaterial.

While $R(r)$ is intuitive, $G(r)$ is the distribution determined directly from experimental data. The form of $G(r)$ in Eq. (1) assumes that the structure factor $S(Q)$ is measured down to a $Q_{\min}\neq 0$, that is, large enough to exclude contributions from small angle scattering (SAS) (Ref. 7) in either x-ray or neutron-scattering experiments, as the second term in $G(r)$, namely, $4\pi r\rho_0$, is the contribution from $S(Q<Q_{\min})$ for bulk materials.[13] Within the small Q region containing the SAS data, scattering is unaffected by the atomic granularity of the density and is thus equal to that for a material of uniform density. The general form of $S(Q<Q_{\min})$ for materials of any shape and size[13] is

$$S(Q) - 1 = \rho_0 \int_0^\infty f(r)\frac{\sin Qr}{Qr} 4\pi r^2 dr. \tag{8}$$

Transforming the SAS data to r space using Eq. (8) gives $4\pi r\rho_0 f(r)$. Knowing that $f(0)=1$, the form of $f(r)$ can thus be found directly from SAS data. If the second term in Eq. (2) is replaced by $4\pi r\rho_0 f(r)$, one finds the general form of

$G(r)$ that fluctuates about zero at large r for materials of all shapes and sizes, namely,

$$G(r) = 4\pi r\rho_0\left[\frac{R(r)}{4\pi r^2\rho_0} - f(r)\right] = 4\pi r\rho_0 f(r)[P(r) - 1]. \tag{9}$$

Solving Eq. (9) for $R(r)$ gives

$$R(r) = rG(r) + 4\pi r^2\rho_0 f(r). \tag{10}$$

Inserting this expression for $R(r)$ into Eq. (7), one gets the expression for the universal RRDF $P(r)$ of the material that can be found directly from experimental data, namely,

$$P(r) = 1 + \frac{G(r)}{4\pi r\rho_0 f(r)}. \tag{11}$$

The first term describes the baseline that represents the homogeneous density limit and the second term describes the fluctuations due to atomic geometry and granularity.

In addition to the finite extent of a material, another experimental limitation that affects the amplitude of the peaks in $G(r)$ is the finite Q-space resolution of the instrument. The finite resolution has the effect of convoluting the true structure factor $S(Q)$ by a resolution function, causing the true $G(r)$ to be multiplied by an envelope function equal to the Fourier transform of the resolution function, thus dampening the peak amplitudes. For example, a Gaussian resolution function causes $G(r)$ to be multiplied by the corresponding Gaussian envelope function and more complex functions can also be used.[14] The finite resolution of the instrument acts on data from bulk materials and nanomaterials alike.

This raises the question of the best way to analyze experimental data and the key decision as to whether to compare theory (including computer simulations) in real space or reciprocal space.[15] There are advantages to both approaches. If the resolution function of the instrument is unknown and has a significant effect on the structure factor $S(Q)$, then there is little choice than to do the comparison in reciprocal space. One way to do this would be to use a RRDF $P(r)$ as in the bulk material and obtain the reduced pair distribution function $G(r)$ via Eq. (9). This requires some assumed form for the shape factor $f(r)$ to be used, which will have to be obtained from microstructural information, small-angle scattering, a plausible guess, etc. Then the structure factor $S(Q)$ can be obtained from the back sine Fourier transform of Eq. (1) and compared to the experiment. The fact that $P(r)$ oscillates about unity at large values of r provides a very useful consistency check on procedures.

If sufficient knowledge of the experimental resolution is available, then the experimental structure factor $S(Q)$ can be resolution corrected, and the reduced pair distribution function $G(r)$ obtained via Eq. (1). One way this can be done is provided by a parameterization scheme given in Ref. 14, which is particularly straightforward if a single Gaussian convolution is involved. The RRDF $P(r)$ is then obtained via Eq. (11), where the resolution function is removed as a multiplicative Gaussian. The form factor $f(r)$ used should be such that at large distances r, the RRDF goes to unity as shown, for example, in the lower panel of Fig. 4. This is a rather strong constraint. The determination of an appropriate shape factor $f(r)$ is facilitated if independent data is available via microstructural studies, small-angle scattering, etc. If there is a distribution of shape factors, due to differences in the sizes and shapes of the nanomaterials, then an ensemble averaged $f(r)$ can be used[13] because $G(r)$ is linear in $f(r)$ from Eq. (9). It should be noted that all this analysis assumes that there are no correlations between the orientation of the nanoparticle boundaries with that of the atomic lattice, that is, the individual nanomaterials act independently and are uncorrelated, and also that there is no matrix material between the nanomaterials. Further refinements to the theory are needed to incorporate such effects.

III. GENERAL PROPERTIES OF THE SHAPE FACTOR

The shape factor $f(r)$ is equal to 1 at all r for a bulk material. For materials with boundaries, $f(r)$ has the general form at small r

$$f(r) = 1 - \frac{S}{4V}r + O(r^2), \tag{12}$$

where S/V is the ratio of surface area to volume for the nanomaterial. The argument is based on consideration of length scales such that the surface is approximately locally flat on these scales.

Let us consider an atom i (more accurately any point) lying at a distance a inside a surface. When we construct $R(r)$ for $r > a$, part of the spherical shell r to $r+dr$ about a point will lie in empty space rather than within the material, and thus the contribution of atom i to $R(r)$ will be less than that of an atom in the bulk. The lost contribution can be quantified in terms of the fraction of the surface area of the sphere of radius r that lies outside of the boundary of the nanomaterial. This "missing" surface area is that of a spherical cap, equal to $2\pi r(r-a)$, while the remaining surface area is $4\pi r^2 - 2\pi r(r-a)$.

We now consider that there will be a missing area contribution in $R(r)$ from all points lying within $0 < a < r$ of the surface. We therefore integrate the missing and remaining contributions. For the missing contribution we have

$$\int_0^r 2\pi(r^2 - ar)da = \pi r^3 \tag{13}$$

and for the remaining contribution

$$\int_0^r [4\pi r^2 - 2\pi r(r-a)]da = 3\pi r^3. \tag{14}$$

The net effect is that we are missing 1/4 of the total contribution to $R(r)$ from points lying within a distance r of the surface. For a nanomaterial of volume V and surface area S, the volume lying within a very small distance r of the surface is rS, which is a fraction rS/V of the total volume of the nanomaterial. Therefore, $R(r)$ for the nanomaterial at small r will be equal to $R_b(r)$, the value for the infinite bulk material, less 1/4 of the contribution from the "surface volume;" so the shape factor $f(r)$ to first order in r is

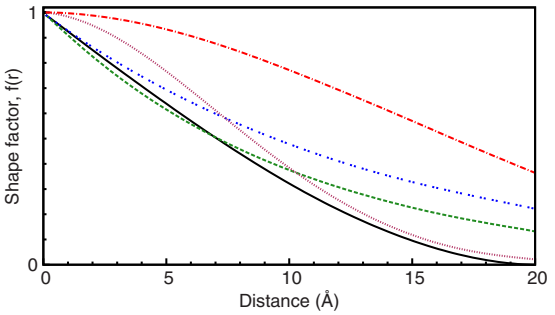

FIG. 2. (Color online) The shape factor for a sphere of radius $a=10$ Å, (black solid) compared with four commonly used shape factors. The Gaussian shape factors have length scales $\sigma=a$ (purple dot) and $\sigma=2a$ (red dot dash) while the exponential shape factors have $\sigma=a$ (green dash) and σ such that the gradient at $r=0$ matches the gradient of $f(r)$ for the sphere (blue double dot).

$$f(r) \simeq 1 - \frac{S}{4V} r. \tag{15}$$

At larger values of r, $f(r)$ will deviate from this linear form as the assumption that the surface is locally flat begins to break down. We can confirm that $f(r)$ for all the shapes we list in this paper (see Appendix) behaves as Eq. (15) at low r. This indicates that $f(r)$ can be similar for solids of different shapes, *e.g.*, different ellipsoids, as the leading term in $f(r)$ depends only on the surface-to-volume ratio S/V. *This suggests a limitation on the amount of shape information that can be obtained from RDF studies on nanomaterials*.

Shape factors that are commonly used are Gaussian $[\exp(-r^2/\sigma^2)]$ and exponential $[\exp(-r/\sigma)]$, where σ is a length scale describing the nanosystem. In Fig. 2 we show $f(r)$ for a sphere of radius $a=10$ Å, for which the analytic form is known (see Appendix) and compare it with two Gaussian and two exponential shape factors. The Gaussian shape factors are shown with $\sigma=a$ and $\sigma=2a$, and of the two exponential shape factors, one has a length scale $\sigma=a$ and the other has the gradient at $r=0$ matched to the gradient of the $f(r)$ for the sphere. None of these functions is a good match to the actual shape of $f(r)$ for the sphere with the Gaussian even lacking the proper linear behavior at small r. The Gaussian and exponential shape factors can also be shown to fail at modeling $f(r)$ of spheroids and other simple geometric shapes. Great caution should therefore be taken when using Gaussian or exponential shape factors in the interpretation of RDF data on nanomaterials.

We note that there is a useful sum rule on the shape factor $f(r)$ for any nanomaterial shape, namely,

$$\int_0^\infty f(r) 4\pi r^2 dr = V_n, \tag{16}$$

where V_n is a volume of a single nanomaterial. This is intuitively clear by recalling that $f(r)$ represents the fraction of the average shell of radius r, that is, within the material. Integrating over all shells thus gives the volume of the nanomaterial. For films, cylinders, etc., discussed in the Appendix, the volume of the nanomaterial would of course be infinite. Combining Eqs. (15) and (16) for the exponential form $\exp(-r/\sigma)$ of the form factor leads to a volume of $8\pi\sigma^3$ and a surface area of $32\pi\sigma^2$ with at least one dimension being infinite in extent. It is unlikely that such a shape of uniform density exists but we will leave this to the reader to investigate further. Thus we recommend that in the absence of any information concerning the shape of the nanomaterials, it is better to use the form for a sphere given in Eq. (A2), with an appropriate choice of the radius a.

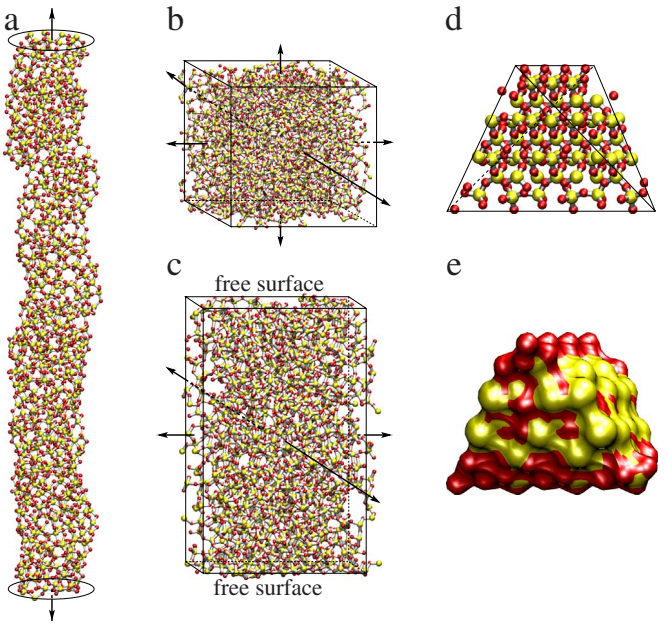

FIG. 3. (Color online) Network models of amorphous silica are shown for (a) a nanorod, (b) bulk, and (c) nanofilm. These models are fully coordinated everywhere, including at the surface, and were created as part of a study on amorphous material (Ref. 16). A crystalline silica network in the shape of a nanotetrahedron is shown in both (d) and (e). In all five figures, silicon and oxygen atoms are colored yellow and red, respectively. Those surfaces subject to periodic boundary conditions are indicated by their normal vectors. In the first four figures, the supercells are outlined with black lines. (d) and (e) represent the same model in the same orientation. (d) shows individual atoms while (e) shows the surface.

IV. RESULTS

Three amorphous silica models were built as part of a study on noncrystalline networks[16] using a modified Wooten, Winer, and Weaire (WWW) approach:[17–19] a bulk, nanofilm, and nanorod model. In the bulk model the cubic supercell is periodic in all three dimensions [Fig. 3(b)]. In the nanofilm model the rectangular supercell is periodic in two dimensions while having two free surfaces along the remaining dimension [Fig. 3(c)]. The model represents an infinitely wide nanomaterial that has a finite thickness. In the rod model the supercell is periodic in only one dimension [Fig. 3(a)] and represents an infinitely long nanomaterial with a roughly circular cross section. In all three models, each silicon and oxygen atom, including those at the surface is, respectively, bonded to four nearest-neighboring oxygen atoms and two nearest-neighboring silicon atoms.[16]

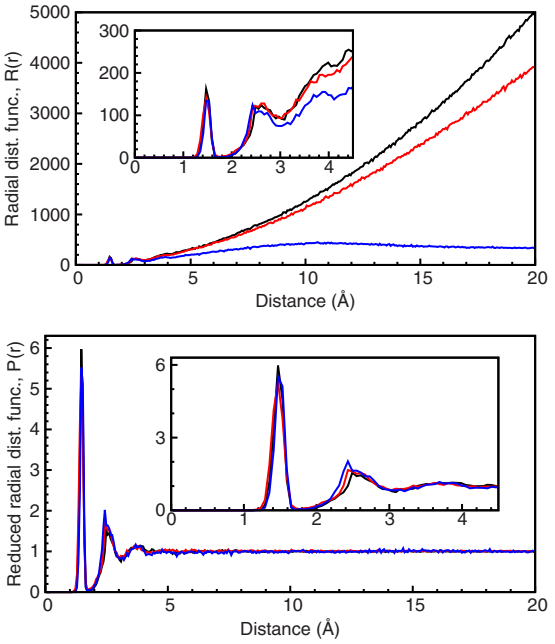

FIG. 4. (Color online) The distance distributions computed according to the RDF (top) and the RRDF (bottom) of the bulk (black), nanofilm (red), and nanorod (blue) amorphous silica network models. The inset figures show closeups at short distances (0–4.5 Å). The atomic numbers are used as weight factors in the computation of the RDF and RRDF.

The three amorphous silica models differ significantly from each other in shape and size. Their RDFs as defined in Eq. (3) differ considerably, as shown in the top panel of Fig. 4. At large distances, the RDFs of the bulk, nanofilm, and nanorod models are proportional to r^2, r, and a constant, respectively, as expected.

We apply Eq. (7) to decouple the intrinsic atomic geometry of the three amorphous silica models from the shape and size effects. The denominator $R^u(r)$ for each model, namely, the RDF of the medium of uniform density having the same shape and size, has an analytical form for the three models. As discussed previously, $R^u(r)=4\pi r^2\rho_0$ for the bulk model. The RDFs $R_b^u(r)$ of an infinitely wide film and an infinitely long cylindrical rod are listed in Eqs. (A3) and (A11), respectively. To the best of the authors' knowledge, the RDF of an infinite uniform cylindrical rod has not previously been found in the concise form derived in the Appendix. By dividing the raw RDF data of the three models displayed in the top panel of Fig. 4 by the appropriate $R^u(r)$, we obtain the RRDFs of the three models, as shown in the bottom panel of Fig. 4.

Independent of the shape and size of the network model, the RRDF reveals the underlying intrinsic atomic geometry with great accuracy. As shown in the bottom panel of Fig. 4, the RRDFs of the bulk, nanofilm, and nanorod are essentially the same. This correctly represents the fact that the three models are virtually indistinguishable from each other in terms of local topology with minor differences due to surface reconstruction and distortion from the ideal geometric shape (the nanorod is not a perfect cylinder, etc.). In all three models, atoms are fully coordinated; bonding networks are amorphous; distortions in bond lengths and bond angles are within narrow ranges.[16] The nanorod model has the widest second peak in its RRDF due to the high fraction of surface atoms that have had their bond angles distorted due to surface reconstruction.

The nanofilm and cylindrical nanorod models are two of the few fortunate cases for which the RDFs $R^u(r)$ of the corresponding uniform media have analytical expressions. For nanomaterials of most shapes, analytical expressions for $R^u(r)$ are not available. In fact it is quite challenging to derive the analytical form of the RDF of almost any geometrical shape, and to date it has not been possible for any shape whose surface contains a singularity, such as an edge or vertex. For example, even for the simplest case, the RDF of a uniform medium in the shape of a cube has not been derived in closed form, although it is easy to write in terms of a double integral that does the spherical averaging.

The computation of the RRDF according to Eq. (7), however, is not hindered by the lack of analytical expressions for RDFs of uniform media. No matter how complicated the shape of a nanomaterial, the RDF of the correspondingly shaped uniform medium can be calculated numerically. As long as the definitions of the "inside" and "outside" of a material are programmable, a large number of distances can be computed between randomly generated pairs of points that lie within the boundary of the shape. The histogram of pair separations is proportional to the RDF of the uniform medium of the same shape and size as the real material. The RRDF of the nanomaterial is then computed according to Eq. (7).

To demonstrate this numerical procedure, we computed the RRDF of a crystalline silica network model in the shape of a regular tetrahedron [Figs. 3(d) and 3(e)]. The nanotetrahedron model is cut out of a bulk crystalline α-quartz network model without further optimization, creating dangling bonds at the surfaces. The edge length of the tetrahedron is chosen to be 28.3 Å. The model is used in this study to exemplify the numerical calculation of an RRDF for an object bounded in all three dimensions. The RRDF is well defined up to the maximum possible separation within the object.

To the best of the authors' knowledge, the analytical form of the RDF of a regular tetrahedron of uniform density has not been derived. We therefore numerically compute the RDF of a uniform tetrahedron using one billion pairs of points to achieve a smooth and well-converged distance distribution. The RRDF of the nanotetrahedron silica network model is then computed according to Eq. (7).

As discussed in Sec. II, expressing $R(r)$ as $R_b(r)f(r)$ is exact only when $R(r)$ is the RDF averaged over nanomaterials representing cuts in all possible locations and orientations with respect to the bulk material, as shown in Fig. 1. If the set of nanomaterials does not represent all possible locations and rotations, the use of the shape factor through Eq. (7) gives only an approximation to the average RDF of the set. The robustness of this approximation is shown in Figs. 5 and 6 by comparing the RDF and RRDF of the bulk material with the average RDF and RRDF of several sets of tetrahedra. These sets include a single tetrahedron, tetrahedra with a single fixed orientation but all possible locations, tetrahedra

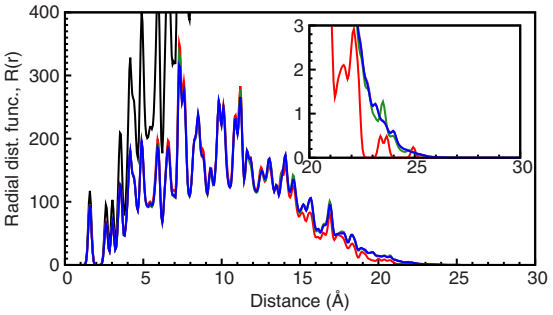

FIG. 5. (Color online) The RDF of a bulk crystalline α-quartz network model (black) compared to the RDF of a single nanotetrahedron silica network model (red). Also included is the average RDF of one million nanotetrahedron silica network models with random locations but fixed orientation (green), fixed location but random orientations (purple, underneath blue), and random locations and orientations (blue). The purple and blue curves are indistinguishable at the resolution plotted. The inset figure shows a closeup over distances from 20 to 30 Å.

with a single fixed location but all possible orientations, and tetrahedra with all possible locations and orientations.

The RRDFs of all four sets show good agreement with the RRDF of the bulk material except at distances that approach the maximum possible pair distance contained within the tetrahedral boundaries. All peaks in the RRDF represent genuine interatomic distance contributions, as the numerically determined RDF of the tetrahedron of uniform density is smooth and nonzero over the relevant distances. The deviations from unity at large distances are amplified in the RRDF relative to the RDF, as $f(r)$ in the denominator of Eq. (7) becomes small at these distances. The small disparity between the average RRDF of the set of tetrahedra with all possible locations and orientations and the RRDF of the bulk (below 28.3 Å) is due only to the computational limitations of sampling a finite number of tetrahedra in the calculation of $R(r)$ and a finite number of pairs in the calculation of $R^u(r)$. Otherwise the agreement would be perfect, as this set represents the complete ensemble of possible tetrahedra. For the other three sets, additional deviations in peak amplitude are due to differences in the frequency that a pair of atoms of a given separation appears in the sets relative to the frequency in the complete ensemble. Some atom pairs from the bulk may be completely absent within a given set of tetrahedra despite having separations below 28.3 Å due to constraints on location and orientation. Averaging over orientation alone results in an RDF that more closely resembles the RRDF of the bulk than does the average over location, although this may not be a general result for nanomaterials of all shapes and sizes, and for materials of all atomic geometries.

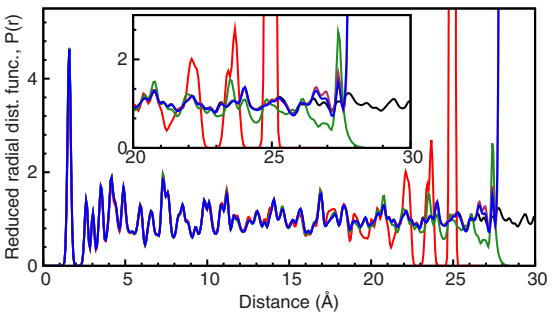

FIG. 6. (Color online) The same distributions as Fig. 5 but plotted as RRDFs. The inset figure shows a closeup over distances from 20 to 30 Å. The largest distance within the nanotetrahedron is the edge length, 28.3 Å.

V. SUMMARY

In this paper we have demonstrated how a shape factor can be used to transform the RDF of finite and bulk material onto a more general function, the RRDF depending only on the intrinsic atomic geometry of the material and not on the shape and size of the nanoparticles. The RRDF will be affected by surface reconstruction and other changes, such as voids, for example, when compared to bulk material with nominally similar atomic structure. The RRDF has a baseline of unity for materials of all atomic geometries and of any shape and size, as illustrated in Figs. 4 and 6, and this is a particularly useful constraint on the data at large r where the oscillations in the RRDF decay. The RRDF keeps the information describing the vital atomic geometry intact so that differences between nanomaterials of various shapes and sizes due to surface relaxation and structural rearrangement can be directly observed, independent of the main size and shape effects. We have shown how to compute the form factor for an arbitrary shape and used the tetrahedral nanoparticles of vitreous silica as an illustration.

ACKNOWLEDGMENTS

We should like to thank S. J. L. Billinge and C. L. Farrow for useful discussions and NSF for support under Grants No. DMR 0703973 and No. DMR 0714953. Some of this work was initiated at the Bellairs Research Institute, Barbados.

APPENDIX: RDF OF UNIFORM MEDIA

For a handful of simple geometrical shapes, the analytical forms of the RDFs of uniform continuous media $R^u(r)$ have been presented in the literature. For the sake of convenience these analytical expressions are listed here and some new expressions added. To save space, all those efforts that express RDFs in integral forms that need further numerical computations are not listed. In all the expressions below, the symbol ρ_0 represents the three-dimensional density.

The RDF of single objects can be found by using the fact that the RDF is the average distribution seen by the units of density within it. Each unit of density observes the same three-dimensional density distribution as does the unit of density at the predefined origin, except that the distribution appears translated due to the difference in viewing locations. Averaging over the observed distributions is equivalent to finding the density-density autocorrelation of the object,[12] as displayed in Fig. 7. The density-density autocorrelation $c(\mathbf{r})$ is a three-dimensional density distribution given by

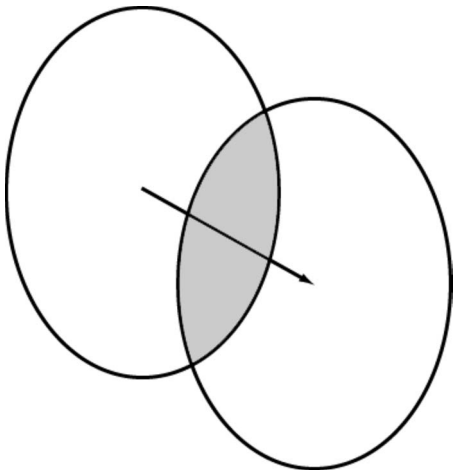

FIG. 7. The probability that two random units of density lying within an object are separated by **r** is proportional to the density-density autocorrelation function of the nanomaterial. In the case of two-dimensional ellipses of uniform density, the autocorrelation is proportional to the area of overlap of two ellipses displaced by the vector **r**. The same area could be found by placing the displacement arrow entirely inside the upper left ellipse and tracing out the possible locations of the arrow tip.

$$c(\mathbf{r}) = \frac{1}{\rho_0 V}\int_{-\infty}^{\infty} \rho(\mathbf{R})\rho(\mathbf{R}+\mathbf{r})d^3R, \tag{A1}$$

where $\rho(\mathbf{r})$ is the three-dimensional density distribution of the object of interest and V is its volume. The autocorrelation is normalized here so as to have a maximum density of ρ_0 at $c(\mathbf{0})$. Note that $c(\mathbf{r})$ is proportional to the probability of finding two units of density within the object with separation **r**. The RDF depends only on the magnitude of **r** and can be found by performing a spherical integration of $c(\mathbf{r})$ about the origin. For objects of uniform density, $R^u(r)=4\pi r^2\rho_0 f(r)$, allowing $f(r)$ to be found directly from the spherical average of $c(\mathbf{r})$.

Applying Eq. (A1) to a single uniform sphere of density ρ_0 and radius a, and dividing by $4\pi r^2\rho_0$ produces the shape factor[11,20–22]

$$f_{sphere}(r) = \begin{cases} \left(1-\frac{r}{2a}\right)^2\left(1+\frac{r}{4a}\right) & r<2a \\ 0 & r>2a. \end{cases} \tag{A2}$$

Similarly, the shape factor of a single uniform infinitely wide film of thickness d has the form[11,16]

$$f_{film}(r) = \begin{cases} 1-\frac{r}{2d} & r<d \\ \frac{d}{2r} & r>d. \end{cases} \tag{A3}$$

The advantage of using the density-density autocorrelation to obtain the RDF over the method used by Kodama *et al.*[11] can be seen, for example, in an *infinitely long uniform cylinder* of radius a. Performing the autocorrelation with the proper normalization, one obtains a three-dimensional distribution with cylindrical symmetry and a radial dependence given by

$$c(p) = \begin{cases} \frac{2}{\pi}\left[\sin^{-1}\sqrt{1-\left(\frac{p}{2a}\right)^2} - \frac{p}{2a}\sqrt{1-\left(\frac{p}{2a}\right)^2}\right] & r<2a \\ 0 & r>2a, \end{cases} \tag{A4}$$

where p is the distance from the axis of symmetry. By choosing a point along the axis as the center for the spherical averaging, p can be expressed as $p=r\sin\theta$, where θ is the angle between **r** and the axis of the cylinder. The spherical average can be expressed as

$$R^u_{cyl}(r) = 8r^2\rho_0\int_0^{\theta_{\max}} \sin\theta \sin^{-1}\sqrt{1-\left(\frac{r}{2a}\right)^2\sin^2\theta}\,d\theta - \frac{4r^3\rho_0}{a}\int_0^{\theta_{\max}} \sin^2\theta\sqrt{1-\left(\frac{r}{2a}\right)^2\sin^2\theta}\,d\theta, \tag{A5}$$

where $\theta_{\max}$ is the angle at which p is maximal for a given r while remaining within the region $p<2a$, where the effective density is larger than zero. For $r<2a$, $\theta_{\max}=\pi/2$, otherwise $\theta_{\max}=\sin^{-1}(2a/r)$. By applying integration by parts to the first term, it becomes

$$8r^2\rho_0\left[\frac{\pi}{2} - \frac{r}{2a}\int_0^{\theta_{\max}} \frac{1-\sin^2\theta}{\sqrt{1-\left(\frac{r}{2a}\right)^2\sin^2\theta}}d\theta\right]. \tag{A6}$$

Substituting Eq. (A6) into Eq. (A5), the RDF of an infinite cylinder can be expressed as a sum of elliptical integrals, namely,

$$R^u_{cyl}(r) = 4\pi r^2\rho_0\left\{1-\frac{8a}{3\pi r}\left[1+\left(\frac{r}{2a}\right)^2\right]E\left(\theta_{\max},\frac{r}{2a}\right) + \frac{8a}{3\pi r}\left[1-\left(\frac{r}{2a}\right)^2\right]F\left(\theta_{\max},\frac{r}{2a}\right)\right\}, \tag{A7}$$

where

$$E(\phi,k) = \int_0^{\phi}\sqrt{1-k^2\sin^2\theta}\,d\theta \tag{A8}$$

$$F(\phi,k) = \int_0^{\phi}\frac{d\theta}{\sqrt{1-k^2\sin^2\theta}} \tag{A9}$$

$$K(k) = \int_0^{\pi/2}\frac{d\theta}{\sqrt{1-k^2\sin^2\theta}}. \tag{A10}$$

For $r<2a$, $\theta_{\max}=\pi/2$ and thus $F(\pi/2,r/2a)=K(r/2a)$. For $r>2a$, the substitution $(r/2a)\sin\theta=\sin\theta'$ allows $F[\sin^{-1}(2a/r),\frac{r}{2a}]$ to be written as $(2a/r)K(2a/r)$. The shape factor $f_{cyl}(r)=R^u_{cyl}(r)/(4\pi r^2\rho_0)$ of an infinite cylinder of radius a thus has the form[16]

$$f_{cyl}(r)=\begin{cases}1-\dfrac{8a}{3\pi r}\left(1+\dfrac{r^2}{4a^2}\right)E\left(\dfrac{\pi}{2},\dfrac{r}{2a}\right)+\dfrac{8a}{3\pi r}\left(1-\dfrac{r^2}{4a^2}\right)K\left(\dfrac{r}{2a}\right) & r<2a\\ 1-\dfrac{8a}{3\pi r}\left(1+\dfrac{r^2}{4a^2}\right)E\left[\sin^{-1}\left(\dfrac{2a}{r}\right),\dfrac{r}{2a}\right]+\dfrac{16a^2}{3\pi r^2}\left(1-\dfrac{r^2}{4a^2}\right)K\left(\dfrac{2a}{r}\right) & r>2a.\end{cases} \tag{A11}$$

To the best of the author's knowledge, the RDF of a infinite cylinder has never been expressed in such a simplified form. The power of the autocorrelation method can be seen by comparing Eq. (A11) to the equivalent result by Kodama *et al.*[11]

For a prolate spheroid whose three axes are a, a, and av, respectively, with $v\geq 1$, the shape factor has the form[12,20]

$$f_{prolate}(r)=\begin{cases}1-\dfrac{3r}{8av}\left(1-\dfrac{r^2}{16a^2}\dfrac{2/3+v^2}{v^2}\right)-\dfrac{3r}{8a}\left(1+\dfrac{r}{4a}\right)\left(1-\dfrac{r}{4a}\right)\dfrac{v}{\sqrt{v^2-1}}\tan^{-1}\sqrt{v^2-1} & 0\leq r\leq 2a\\ 1-\dfrac{3r}{8av}\left(1-\dfrac{r^2}{16a^2}\dfrac{2/3+v^2}{v^2}\right)-\dfrac{3}{8}\left(1+\dfrac{r^2}{8a^2}\right)\sqrt{1-\dfrac{4a^2}{r^2}}\dfrac{v}{\sqrt{v^2-1}} & \\ \quad-\dfrac{3r}{8a}\left(1+\dfrac{r}{4a}\right)\left(1-\dfrac{r}{4a}\right)\dfrac{v}{\sqrt{v^2-1}}\left(\tan^{-1}\sqrt{v^2-1}-\tan^{-1}\sqrt{\dfrac{r^2}{4R^2}-1}\right) & 2a\leq r\leq 2av.\end{cases} \tag{A12}$$

For an oblate spheroid whose three axes are a, a, and av, respectively, with $v\leq 1$, the shape factor has the form[12,20]

$$f_{oblate}(r)=\begin{cases}\left[1-\dfrac{3r}{8av}\left(1-\dfrac{r^2}{16a^2}\dfrac{2/3+v^2}{v^2}\right)-\dfrac{3r}{8a}\left(1+\dfrac{r}{4a}\right)\left(1-\dfrac{r}{4a}\right)\dfrac{v}{\sqrt{1-v^2}}\tanh^{-1}\sqrt{1-v^2}\right] & 0\leq r\leq 2av\\ \dfrac{v}{\sqrt{1-v^2}}\left[\dfrac{3a}{4r}\left(1+\dfrac{r^2}{8a^2}\right)\sqrt{1-\dfrac{r^2}{4a^2}}-\dfrac{3r}{8a}\left(1+\dfrac{r}{4a}\right)\left(1-\dfrac{r}{4a}\right)\tanh^{-1}\sqrt{1-\dfrac{r^2}{4a^2}}\right] & 2av\leq r\leq 2a.\end{cases} \tag{A13}$$

For a spherical shell of radius a and thickness δ, the shape factor in the range of $0\leq r\leq 2a+\delta$ has the form[14,20]

$$\begin{aligned}f_{shell}(r)=\frac{\pi r\rho_0}{2(12a^2+\delta^2)}\{&r[16a^3+12a\delta(\delta-r)+36a^2(2\delta-r)+3(\delta-r)^2(2\delta+r)]+2(\delta-r)^2[r(2\delta+r)-12a^2]\mathrm{sg}(\delta-r)\\&-2(2a-r)^2[r(4a+r)-3\delta^2]\mathrm{sg}(2a-r)+r(4a-2\delta+r)(2a-\delta-r)^2\mathrm{sg}(2a-\delta-r)\},\end{aligned} \tag{A14}$$

where $\mathrm{sg}(x)=1$ if $x>0$ and -1 if $x<0$.

[1] P. Attard, *Thermodynamics and Statistical Mechanics: Equilibrium by Entropy Maximisation* (Academic, New York, 2002).
[2] B. E. Warren, *X-Ray Diffraction* (Dover, New York, 1990).
[3] M. Wachhold, K. Kasthuri Rangan, M. Lei, M. F. Thorpe, S. J. L. Billinge, V. Petkov, J. Heising, and M. G. Kanatzidis, J. Solid State Chem. **152**, 21 (2000).
[4] E. S. Božin, G. H. Kwei, H. Takagi, and S. J. L. Billinge, Phys. Rev. Lett. **84**, 5856 (2000).
[5] V. Petkov, S. J. L. Billinge, J. Heising, and M. G. Kanatzidis, J. Am. Chem. Soc. **122**, 11571 (2000).
[6] A. Guinier, *X-Ray Diffraction in Crystals, Imperfect Crystals, and Amorphous Bodies* (W. H. Freeman, San Francisco, 1963).
[7] O. Glatter and O. Kratky, *Small Angle X-Ray Scattering* (Academic, London, New York, 1982).
[8] D. B. Williams and C. B. Carter, *Transmission Electron Microscopy: A Textbook for Materials Science* (Plenum, New York, 1996).
[9] D. A. Keen, J. Appl. Crystallogr. **34**, 172 (2001).
[10] V. A. Levashov, S. J. L. Billinge, and M. F. Thorpe, Phys. Rev. B **72**, 024111 (2005).
[11] K. Kodama, S. Iikubo, T. Taguchi, and S. Shamoto, Acta Crystallogr., Sect. A: Found. Crystallogr. **62**, 444 (2006).
[12] B. Gilbert, J. Appl. Crystallogr. **41**, 554 (2008).
[13] C. L. Farrow and S. J. L. Billinge, Acta Crystallogr., Sect. A: Found. Crystallogr. **65**, 232 (2009).
[14] M. F. Thorpe, V. A. Levashov, M. Lei, and S. J. L. Billinge, *From Semiconductors to Proteins: Beyond the Average Structure* (Kluwer Academic, New York, 2002), pp. 105–128.
[15] T. Egami and S. J. L. Billinge, *Underneath the Bragg Peaks: Structural Analysis of Complex Materials* (Pergamon, New York, 2003).
[16] M. Lei, Ph.D. thesis, Michigan State University, 2003.
[17] F. Wooten, K. Winer, and D. Weaire, Phys. Rev. Lett. **54**, 1392 (1985).
[18] F. Wooten and D. Weaire, Solid State Phys. **40**, 1 (1987).
[19] B. R. Djordjevic, M. F. Thorpe, and F. Wooten, Phys. Rev. B **52**, 5685 (1995).
[20] J. J. Muller, S. Hansen, and H. V. Purschel, J. Appl. Crystallogr. **29**, 547 (1996).
[21] D. Schleef, M. Parry, S. J. Tu, B. Woodahl, and E. Fischbach, J. Math. Phys. **40**, 1103 (1999).
[22] R. C. Howell, T. Proffen, and S. D. Conradson, Phys. Rev. B **73**, 094107 (2006).